PERGAMON

Available online at www.sciencedirect.com
SCIENCE DIRECT®

Polyhedron 22 (2003) 2267–2271

POLYHEDRON
www.elsevier.com/locate/poly

$[Mn_{18}]^{2+}$ and $[Mn_{21}]^{4+}$ single-molecule magnets

E.C. Sañudo[a], E.K. Brechin[b], C. Boskovic[b], W. Wernsdorfer[c], J. Yoo[d], A. Yamaguchi[e], T.R. Concolino[f], K.A. Abboud[a], A.L. Rheingold[f], H. Ishimoto[e], D.N. Hendrickson[d],*, G. Christou[a],*

[a] Department of Chemistry and Center for X-ray Crystallography, University of Florida, Gainesville, FL 32611-7200, USA
[b] Department of Chemistry, Indiana University, Bloomington, IN 47405-7102, USA
[c] Laboratoire Louis Néel-CNRS, 38042 Grenoble Cedex 9, France
[d] Department of Chemistry, University of California at San Diego, La Jolla, CA 92093-0358, USA
[e] Institute for Solid State Physics, University of Tokyo, 7-22-1 Roppongi, Minatoku, Tokyo 106-8666, Japan
[f] Department of Chemistry, University of Delaware, Newark, DE 19716, USA

Received 7 October 2002; accepted 28 November 2002

Abstract

The synthesis and structural characterization of the two new Mn complexes $[Mn_{18}O_{14}(O_2CMe)_{18}(hep)_4(hepH)_2(H_2O)_2](ClO_4)_2$ (**1**) and $[Mn_{21}O_{16}(O_2CMe)_{16}(hmp)_6(hmpH)_2(pic)_2(py)(H_2O)](ClO_4)_4$ (**3**) are presented, together with a detailed study of their magnetic properties. Complex **1** possesses a ground-state spin of $S = 13$, and the ground-state spin for **3** is estimated to be $S = 17/2$ or $19/2$. Both complexes **1** and **3** are new examples of single-molecule magnets (SMMs), displaying frequency-dependent out-of-phase AC signals, as well as magnetization vs. DC field hysteresis at temperatures below 1 K. Complex **1** straddles the classical/quantum interface by also displaying quantum tunneling of the magnetization (QTM).

Keywords: Hysteresis; Mn clusters; Quantum tunneling; Single-molecule magnets

1. Introduction

Many present and future specialized applications of magnets require monodisperse, nanoscale magnetic particles, and the discovery that individual molecules can function as nanoscale magnets was thus a significant development [1–3]. Such a molecule, named as single-molecule magnet (SMM), functions as a single-domain magnetic particle that, below its blocking temperature, exhibits the classical property of a magnet, namely, magnetization hysteresis. In addition, it straddles the classical/quantum interface in also displaying quantum tunneling of magnetization (QTM) [4] and quantum phase interference [5]. An SMM derives its unusual properties from a combination of large spin (S) and large, easy-axis-type anisotropy (negative axial zero field splitting (ZFS) parameter D). These result in a significant barrier to thermally activated magnetization relaxation, with upper limits given by $S^2|D|$ or $(S^2-1/4)|D|$ for integer and half-integer spin, respectively. The first SMM was $[Mn_{12}O_{12}(O_2CMe)_{16}(H_2O)_4]$ [1–3] with $S = 10$ and $D = -0.50\ cm^{-1} = -0.72$ K. Since then, other oxidation levels of the $[Mn_{12}]$ family [6] and other Mn_x and M_x (M = Fe, Co, V or Ni) SMMs have been prepared with various S values, both integer and half-integer [7]. Recently, the first exchanged-coupled dimer of SMMs has demonstrated the feasibility of fine-tuning the quantum properties of these nanoscale magnetic materials [8].

We present here two new SMMs of high nuclearity and large spin, containing the ligands 2-hydroxymethylpyridine (hmpH) and 2-(2-hydroxyethyl)pyridine (hepH).

---

* Corresponding author.

0277-5387/03/$ - see front matter © 2003 Elsevier Science Ltd. All rights reserved.
doi:10.1016/S0277-5387(03)00204-3

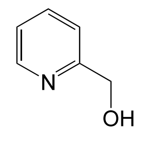

hmpH

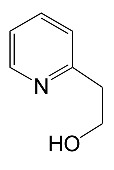

hepH

2. Results and discussion

2.1. Preparation of compounds

$[Mn_{18}O_{14}(O_2CMe)_{18}(hep)_4(hepH)_2(H_2O)_2](ClO_4)_2$ (**1**) was prepared as previously described [9]. $[Mn_{21}O_{16}(O_2CMe)_{16}(hmp)_6(hmpH)_2(pic)_2(py)(H_2O)](ClO_4)_4$ (**3**) was prepared by treating a solution of $[Mn_{10}O_4(OH)_4(O_2CMe)_8(hmp)_8](ClO_4)_4$ (**2**) [10] in MeCN with 3 equiv. of $[Mn_3O(O_2CMe)_6(py)_3]ClO_4$ [11]. Layering of the reaction mixture with Et_2O afforded crystals of **3** after 3–4 weeks. Both **1** and **3** contain Mn in the oxidation states Mn^{II} and Mn^{III} (vide infra), even though they both can be prepared from starting materials containing exclusively Mn^{III}. The synthesis of **1** can be optimized using a mixture of starting materials containing Mn^{II} and Mn^{III}, making unnecessary a redox process. For complex **3**, the redox process is absolutely necessary, since it leads to the formation of the two picolinate ligands in the cluster by oxidation of hmp^-.

2.2. X-ray crystallography

Complexes **1**·6MeCN crystallizes in the triclinic space group $P\bar{1}$. There is one Mn_{18} per unit cell, lying at a center of inversion. For the sake of brevity, references to atoms in the following discussion implicitly include their symmetry related partners. Pov-Ray representations of the cores of **1**·6MeCN and **3**·xMeCN are shown in Figs. 1 and 2. The structure of **1** consists of an $[Mn_{18}(\mu_4\text{-}O)_4(\mu_3\text{-}O)_{12}(\mu_2\text{-}O)_8]^{4+}$ core. The core can be described as a nearly linear central Mn_4O_6 unit (Mn_1 and Mn_6), to either side of which there is a Mn_7O_9 unit. This side unit can be envisioned as a distorted cubane and two distorted cuboids (i.e. apically deficient cubanes) which are face sharing. The side units are attached to the central Mn_4O_6 by the six triply bridging oxides (O21, O24 and O25), and by the two hepH ligands (O27). Only 14 of the oxygens in the core are O^{2-}, the rest are part of the carboxylates and hep^-/hepH ligands. The four μ_4-O (O22 and O23) and 10 of the 12 μ_3-O (O19, O20, O21, O24 and O25) are from oxo ligands. The other two μ_3-O atoms (O10) are from acetate ligands binding in the extremely rare η^1:η^3:μ_4 bridging mode. Of the eight μ_2-O atoms, six (O26, O27 and O28) are associated with the six hep^-/hepH ligands; the remaining μ_2-O (O4) are from acetate ligands binding in a η^1:η^2:μ_3 manner. Bond valence sums [12] and Jahn-Teller elongation axes establish a $2Mn^{II}$, $16Mn^{III}$ trapped-valence oxidation state description, with Mn9 being the Mn^{II} ions. There are two perchlorates acting as counterions; thus, the charge balance requires two of the carboxylates or chelating ligands to be protonated. Close examination of metric parameters reveals O27 to be protonated, as well as O29 to be part of a water molecule. All of the Mn^{III} ions display JT elongation axes roughly perpendicular to the plane of the molecule, except Mn7, which has a JT axis oriented perpendicular to all of the other JT axes. The observed bond distances and angles are in agreement with what is expected for Mn^{II} and Mn^{III} in the described geometry, with the exception of the long 2.5 Å distance for Mn6–O27.

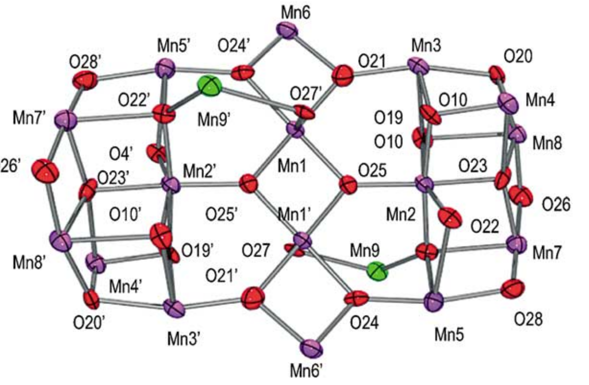

Fig. 1. Pov-Ray plot ORTEP at the 50% level of probability of the core of $[Mn_{18}O_{14}(O_2CMe)_{18}(hep)_4(hepH)_2(H_2O)_2](ClO_4)_2$ (**1**).

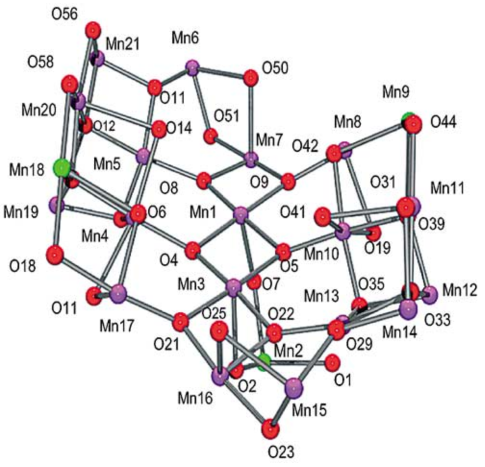

Fig. 2. Pov-Ray ORTEP plot at the 50% level of probability of the cation of $[Mn_{21}O_{16}(O_2CMe)_{16}(hmp)_6(hmpH)_2(pic)_2(py)(H_2O)](ClO_4)_4$ (**3**).

Complex **3** crystallizes in the triclinic space group $P\bar{1}$. There are two Mn_{21} units per unit cell and each of these consists of a $[Mn_{21}(\mu_4\text{-}O)_4(\mu_3\text{-}O)_{12}(\mu_2\text{-}O)_{16}]$ core. The four of the μ_4-O (O12, O15, O33 and O39) and the 12 of the μ_3-O (O4, O5, O8, O9, O11, O13, O17, O21, O22, O29, O35 and O42) come from oxo ligands. Two μ_2-O are part of the pic$^-$ ligands (O2 and O7), four are from η^1:η^2:μ_3 acetates (O14, O16, O25, O41, O43 and O50) and the last eight are provided by hmp$^-$/hmpH ligands (O18, O23, O32, O44, O45, O51, O56 and O58). The core of **3** is structurally related with that of **1**. It contains the central Mn_4O_6 unit, on each side of this there is an Mn_8O_{11} unit. The two side units can be described as a central Mn_4O_4 cubane sharing two of its faces with two cuboids, one of which is sharing a face with a third cuboid and the other is bound by one of its oxides (O29) to an Mn_2O_2 unit that includes one of the Mn in the central Mn_4O_6 unit (Mn16 and Mn7). The side units are oriented as if there were a C_2 rotation axis lying at the center of the molecule, although there is no such crystallographic symmetry. The molecule is capped by a Mn^{II} (Mn2) that is linked to the central Mn_4O_6 unit by two picolinate anions; this pins the core into an open V shape, with the Mn^{II} at the bottom of the V. Close examination of the metric parameters and bond valence sums indicate the trapped-valence $Mn^{II}_3\,Mn^{III}_{18}$ oxidation state for the complex. Two of the Mn^{II} are part of two of the side units (Mn9 and Mn18) and the third one caps the whole molecule (Mn2). As for **1**, not all the JT axes are parallel. This fact is important to the magnetic properties of **3**, since it reduces the axial anisotropy. Four ClO_4^- counterions are seen in the crystal structure. This was confirmed by chlorine analyses on the sample, which gave $4ClO_4^-$ per cation. Bond valence sums were also performed on the oxygen atoms and it was found that there are two protonated hmpH ligands, as needed for charge balance.

2.3. Magnetic susceptibility studies[1]

2.3.1. Complex $[Mn_{18}O_{14}(O_2CMe)_{18}(hep)_4(hepH)_2(H_2O)_2](ClO_4)_2$ (1)

The ground-state spin of **1** was determined by solid-state magnetization measurements in the 2.0–4.0 K and 2–5 T ranges. The data were fit by diagonalization of the spin Hamiltonian matrix using a full powder-average method that assumes only the ground state is populated and incorporates axial ZFS ($D\hat{S}_z^2$) and Zeeman interactions. The best fit of the data gave $S = 13$, $D = -0.13$ cm^{-1} = -0.19 K, and $g = 1.86$. Although a few higher spin values are known, $S = 13$ is nevertheless an unusually large spin for a molecular species. Its calculated (maximum) barrier to magnetization relaxation is $S^2|D| = 32$ cm^{-1} = 46 K, suggesting **1** might be a new SMM. This was therefore investigated. AC susceptibility data were collected in the 0.04–4.0 K temperature range at nine frequencies from 1.1 to 996 Hz. As the in-phase magnetic susceptibility $\chi'_M T$ decreases, the appearance of a frequency-dependent out-of-phase χ''_M peak is observed in the 0.99–1.44 K region, shown in Fig. 3. This indicates the superparamagnet-like slow relaxation of an SMM. To confirm this, magnetization vs. applied DC field data were collected down to 0.04 K using a micro-SQUID instrument (Fig. 4). Hysteresis loops were observed below 1 K whose coercitivities increase with decreasing T, as expected for an SMM. The loops do not show the step-like features indicative of QTM, but it is possible that steps are present but smeared out by broadening effects from dipolar and transverse fields and/or a distribution of molecular environments. To probe whether complex **1** is undergoing QTM and to determine the effective barrier to magnetization relaxation (U_{eff}), DC magnetization decay data were collected (i) on a microcrystalline sample using a SHE-RLM bridge where a SQUID serves as a null detector; a field

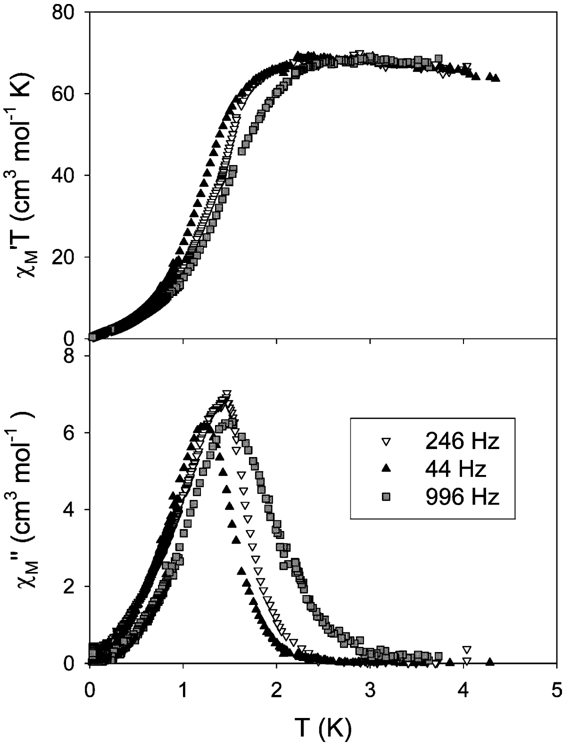

Fig. 3. Plots of $\chi'_M T$ vs. T (top) and χ''_M vs. T (bottom) for complex **1**.

---

[1] Direct current magnetic susceptibility data on powdered microcrystalline sample (restrained in eicosane to prevent torquing at high fields) were collected on Quantum Design MPMS-XL or MPMS SQUID magnetometers equipped with 7 and 5.5 T magnets, respectively. Alternate current magnetic susceptibility measurements were performed with an MPMSXL SQUID magnetometer equipped with a 7 T magnet. Low-temperature magnetic data were collected at the Institute of Solid State Physics, University of Tokyo. Measurements were made on a SHE-RLM bridge where a SQUID served as null detector. The microcrystalline sample was attached onto a quartz glass with Apiezon grease to reduce the background signal. The sample was immersed in non-magnetic liquid ^{4}He. Low-temperature studies on single crystals were performed using an array of micro-SQUIDS. The high sensitivity of this magnetometer allows the study of single crystals of SMMs of the order of 10–500 μm.

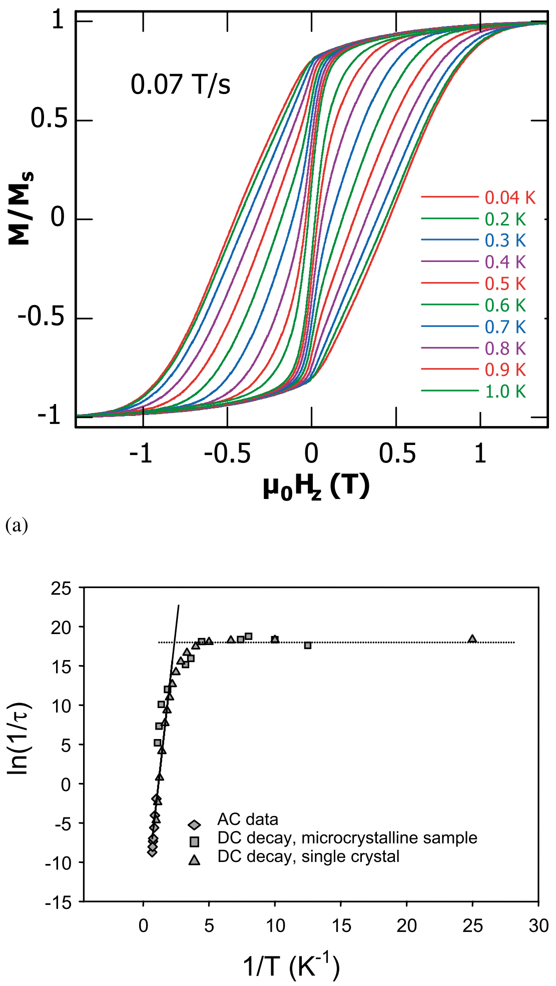

(a)

(b)

Fig. 4. (a) Magnetization vs. field hysteresis loops for **1** at a scan rate of 0.07 T and the indicated temperatures and (b) Arrhenius plot for **1** using AC χ'_M data, and DC decay data on single crystal and microcrystalline samples. The solid line is the fit of the data in the thermally activated region, and the dashed line is the fit of the T-independent data.

of 3.7 G was applied and after temperature equilibration, the field was removed and the magnetization measured as a function of time at 11 temperatures in the 0.910–0.080 K range, with data collection times up to 10^5 s at 0.080 K and (ii) on a single crystal at 16 temperatures in the 0.040–1.00 K range using a micro-SQUID instrument. Each of the 27 datasets was analyzed to give a relaxation time (τ).

The DC decay and AC χ'_M data were combined and used to construct an Arrhenius plot of ln(τ) vs. $1/T$ (Fig. 5). Between 3.5 and 0.50 K, the relaxation rate is temperature-dependent with $U_{\mathrm{eff}} = 14.8$ cm^{-1} = 21.3 K, likely as a result of a thermally activated (Orbach) process [13]. However, below approximately 0.25 K, the relaxation rate is temperature-independent at 1.3×10^{-8} s^{-1}, indicative of QTM between the lowest energy $M_s = \pm 13$ levels of the $S = 13$ state. Such temperature-independent relaxation rates have been reported previously for only a few SMMs [14].

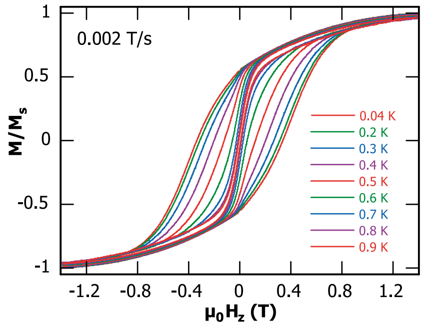

Fig. 5. Magnetization vs. field hysteresis loops for **3** at 0.002 T and the indicated temperatures.

2.3.2. *Complex [$Mn_{21}O_{16}(O_2CMe)_{16}(hmp)_6(hmpH)_2$-$(pic)_2(py)(H_2O)](ClO_4)_4$ (3)*

DC magnetic susceptibility studies on a sample of **3** were performed at an applied field of 1 T. The $\chi_M T$ has a value of 52 cm^3 mol^{-1} K at 300 K and it slightly decreases at 50 K until it reaches a plateau at a value of 38 cm^3 mol^{-1} K. Below 10 K a sudden drop of $\chi_M T$ is observed. $\chi_M T$ suggests a large ground-state spin for complex **3**. AC magnetic susceptibility data were collected in the 1.8–6.0 K range at four frequencies from 10 to 997 Hz. A frequency-dependent out-of-phase signal is observed at T below 2.5 K. As χ'_M increases, a decrease in $\chi'_M T$ is observed, as would be expected for an SMM. To confirm this, magnetization vs. applied DC field data were collected down to 0.04 K using a micro-SQUID instrument. Hysteresis loops were observed below 1 K whose coercitivities increase with decreasing T (Fig. 5), again as expected for an SMM. As for **1**, the loops do not show the step-like features indicative of QTM. Due to the existence of low lying excited states, DC measurements were not useful and a reduced magnetization plot would only give an estimate of the ground-state spin of **3**. Thus, the ground-state spin of **3** was obtained from the in-phase value of the AC magnetic susceptibility. Before its sharp decrease at T below 2.0 K, $\chi'_M T$ has an essentially constant value of ~40 cm^3 mol^{-1} K. This value is consistent with $S = 17/2$ with $g = 1.99$ or $S = 19/2$ with $g = 1.8$. DC decay data on a single crystal were collected and used to construct an Arrhenius plot, shown in Fig. 6. The dashed line is the best fit using the Arrhenius equation, which gave $\tau_o = 7.8 \times 10^{-7}$ s and $U_{\mathrm{eff}} = 11.3$ K.

3. Conclusions

The ligands hepH and hmpH have been used to synthesize the two new SMMs [$Mn_{18}O_{14}(O_2CMe)_{18}(hep)_4$(hepH)$_2(H_2O)_2$]$(ClO_4)_2$ (**1**) and [$Mn_{21}O_{16}$(O$_2$C-

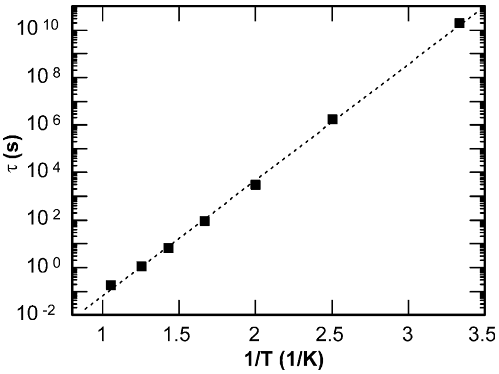

Fig. 6. Arrhenius plot for complex **3** using DC decay data collected on a single crystal. The dashed line is the best fit of the data.

Me)$_{16}$(hmp)$_6$(hmpH)$_2$(pic)$_2$(py)(H$_2$O)](ClO$_4$)$_4$ (**3**). They both contain Mn in the oxidation states Mn^{II} and Mn^{III}. Compounds **1** and **3** are amongst the largest spin and size SMMs to be discovered. In addition, complex **1** is both the largest spin and highest nuclearity SMM to exhibit QTM.

4. Supplementary material

Crystallographic data for the structural analysis have been deposited with the Cambridge Crystallographic Data Centre, CCDC Nos. 193107 and 203152 for compounds **1** and **3**, respectively. Copies of this information may be obtained free of charge from The Director, CCDC, 12 Union Road, Cambridge CB2 1EZ, UK (Fax: +44-1223-336033; e-mail: deposit@ccdc.cam.uk or http://www.ccdc.cam.ac.uk).

Acknowledgements

This work was supported by NSF grants to G.C. and D.N.H.

References

[1] G. Christou, D. Gatteschi, D.N. Hendrickson, R. Sessoli, MRS Bull. 25 (2000) 66.
[2] R. Sessoli, H.L. Tsai, A.R. Schake, S. Wang, J.B. Vincent, K. Folting, D. Gatteschi, G. Christou, D.N.H. Hendrickson, J. Am. Chem. Soc. 115 (1993) 1804.
[3] R. Sessoli, D. Gatteschi, A. Caneschi, M.A. Novak, Nature 365 (1993) 141.
[4] J.R. Friedman, M.P. Sarachik, J. Tejada, R. Ziolo, Phys. Rev. Lett. 76 (1996) 3830.
[5] W. Wernsdorfer, R. Sessoli, Science 284 (1999) 133.
[6] (a) H.J. Eppley, H.L. Tsai, N. de Vries, K. Folting, G. Christou, D.N. Hendrickson, J. Am. Chem. Soc. 117 (1995) 301;
(b) M. Soler, W.K. Chandra, D. Ruiz, E.R. Davidson, D.N. Hendrickson, G. Christou, Chem. Commun. (2000) 2417.
[7] (a) D.N. Hendrickson, G. Christou, H. Ishimoto, J. Yoo, E.K. Brechin, A. Yamaguchi, E.M. Rumberger, S.M. Aubin, Z. Sun, G. Aromi, Polyhedron 20 (2001) 1479;
(b) C. Boskovic, E.K. Brechin, W.E. Streib, K. Folting, J.C. Bollinger, D.N. Hendrickson, G. Christou, J. Am. Chem. Soc. 124 (2002) 3725;
(c) M. Soler, E. Rumberger, K. Folting, D.N. Hendrickson, G. Christou, Polyhedron 20 (2001) 1365;
(d) C. Cadiou, M. Murrie, C. Paulsen, V. Villar, W. Wernsdorfer, R.E.P. Wimpeny, Chem. Commun. (2001) 2666.
[8] W. Wernsdorfer, N. Aliaga-Alcalde, D.N. Hendrickson, G. Christou, Nature 416 (2002) 406.
[9] E.K. Brechin, C. Boskovic, W. Wernsdorfer, J. Yoo, A. Yamaguchi, E.C. Sañudo, T.R. Concolino, A.L. Rheingold, H. Ishimoto, D.N. Hendrickson, G. Christou, J. Am. Chem. Soc. 124 (2002) 9710.
[10] M.A. Bolcar, Doctoral Thesis, Indiana University, 1996.
[11] J.B. Vincent, H.-R. Chang, K. Folting, J.C. Huffman, G. Christou, D.N. Hendrickson, J. Am. Chem. Soc. 109 (1987) 5703.
[12] (a) G. Palenik, Inorg. Chem. 36 (1997) 4888;
(b) W. Liu, H.H. Thorp, Inorg. Chem. 32 (1993) 4102;
(c) I.D. Brown, G. Altermatt, Acta Crystallogr, Sect. B 41 (1985) 244.
[13] A. Abragam, B. Bleaney, Electron Paramagnetic Resonance of Transition Ions, Dover, Mineola, NY, 1986.
[14] (a) H.J. Eppley, H.L. Tsai, N. de Vries, K. Folting, G. Christou, D.N. Hendrickson, J. Am. Chem. Soc. 115 (1993) 1804;
(b) C. Cadiou, M. Murrie, C. Paulsen, V. Villar, W. Wernsdorfer, R.E.P. Wimpeny, Chem. Commun. (2001) 2666.;
(c) C. Sangregorio, T. Ohm, C. Paulsen, R. Sessoli, D. Gatteschi, Phys. Rev. Lett. 78 (1997) 4645;
(d) S.M. Aubin, N.R. Dilley, L. Pardi, J. Krzystek, M.J. Wemple, L.C. Brunel, G. Christou, D.N. Hendrickson, J. Am. Chem. Soc. 120 (1998) 4991.